Biotechnology Advances 34 (2016) 740–753

Contents lists available at ScienceDirect

Biotechnology Advances

journal homepage: www.elsevier.com/locate/biotechadv

Research review paper

Powder-based 3D printing for bone tissue engineering

G. Brunello [a], S. Sivolella [a,*], R. Meneghello [b], L. Ferroni [c], C. Gardin [c], A. Piattelli [d], B. Zavan [c,*], E. Bressan [a]

[a] University of Padova, Department of Neurosciences, Section of Dentistry, Via Giustiniani 2, 35129 Padova, Italy
[b] University of Padova, Department of Management and Engineering, Stradella S. Nicola 3, 36100 Vicenza, Italy
[c] University of Padova, Department of Biomedical Sciences, Via Ugo Bassi 58/B, 35131 Padova, Italy
[d] University of Chieti-Pescara, Department of Medical, Oral and Biotechnological Sciences, Via dei Vestini 31, 66100 Chieti, Italy

ARTICLE INFO

Article history:
Received 8 February 2016
Received in revised form 20 March 2016
Accepted 27 March 2016
Available online 13 April 2016

Keywords:
3D printing
Bone
Scaffold
Additive manufacturing technologies
Powder
Binder
Depowdering
Sintering

ABSTRACT

Bone tissue engineered 3-D constructs customized to patient-specific needs are emerging as attractive biomimetic scaffolds to enhance bone cell and tissue growth and differentiation.
The article outlines the features of the most common additive manufacturing technologies (3D printing, stereolithography, fused deposition modeling, and selective laser sintering) used to fabricate bone tissue engineering scaffolds. It concentrates, in particular, on the current state of knowledge concerning powder-based 3D printing, including a description of the properties of powders and binder solutions, the critical phases of scaffold manufacturing, and its applications in bone tissue engineering. Clinical aspects and future applications are also discussed.

Contents

* Corresponding authors.
E-mail addresses: giulia-bru@libero.it (G. Brunello), stefano.sivolella@libero.it (S. Sivolella), roberto.meneghello@unipd.it (R. Meneghello), letizia.ferroni@unipd.it (L. Ferroni), chiara.gardin@unipd.it (C. Gardin), apiattelli@unich.it (A. Piattelli), barbara.zavan@unipd.it (B. Zavan), eriberto.bressan@unipd.it (E. Bressan).

http://dx.doi.org/10.1016/j.biotechadv.2016.03.009
0734-9750/

1. Introduction

Reconstruction of complex bone defects continues to pose a considerable challenge in patients with inadequate vertical and horizontal bone dimensions requiring alveolar bone augmentation to enable dental implant placement (Tonetti and Hämmerle, 2008; Chiapasco and Zaniboni, 2009). While autogenous bone grafts harvested from intra- or extra-oral sites are still generally considered the gold standard for bone repair, their use is limited in clinical practice given high donor site morbidity and graft resorption rates and circumscribed bone availability (Felice et al., 2009a, 2009b; Araújo et al., 2002; Chiapasco et al., 2007).

Some natural and synthetic biocompatible bone substitutes have been developed to promote bone regeneration as alternatives to autogenous bone grafts (Esposito et al., 2009).

Bone tissue engineering has, moreover, emerged as a promising approach to bone repair and reconstruction (Rezwan et al., 2006, Gardin et al., 2015; Fiocco et al., 2015; Bressan et al., 2013, 2014; Sivolella et al., 2012; Gardin et al., 2012; Kumar et al., 2016a).

Scaffolds play a crucial role in bone tissue engineering. Scaffolds are biocompatible structures of natural or synthetic origin, which can mimic the extracellular matrix of native bone and provide a tridimensional (3D) environment in which cells become attached and proliferate. An ideal scaffold should be biocompatible, biodegradable and have adequate physical and mechanical properties. Interconnected porosity of the scaffold allows cell spreading and effective transport of nutrients, oxygen, waste, as well as growth factors, favouring continuous ingrowth of bone tissue from the periphery into the inner part of the scaffold. Finally, a scaffold should be replaced by regenerative tissue, while retaining the shape and form of the final tissue structure (Zavan et al., 2011; Ferroni et al., 2015; Bose et al., 2013).

Although bone regeneration procedures have taken great strides in recent decades (Esposito et al., 2009), one of the primary challenges that remains is optimizing predictable patient-specific treatment strategies.

Bone blocks must fit into anatomical bone defects. Usually cut and shaped manually at the time of surgery to fit the bone defect and to guarantee the graft's mechanical stability, the process of creating bone blocks is a long and complex one (Markiewicz and Bell, 2011; Smith et al., 2007; Oka et al., 2010). Anatomically shaped bone blocks can be fabricated using computer-aided design and computer aided manufacturing (CAD/CAM) technology that mills scaffolds into the exact shape of the bone reconstruction (Oka et al., 2010; Mangano et al., 2014). The porous architecture of the scaffold is thought to mimic cancellous bone structures thus providing an optimal environment for stem cell spreading and differentiation (Gardin et al., 2012; Bressan et al., 2013).

Additive manufacturing (AM), which refers to various processes including three-dimensional printing (3DP), is a fabrication method using 3D multi-layered constructs to build porous biocompatible scaffolds of pre-defined shapes with excellent mechanical and osteoconductive properties (Vaezi et al., 2013). AM technologies, also known as Rapid Prototyping (RP) or Solid Free-form Fabrication (SFF) techniques, have been receiving considerable attention in view of the fact that customized patient-specific 3D bone substitutes can be manufactured for bone tissue regeneration procedures. The combined use of 3D image analysis and computed tomography (CT) techniques can provide components that precisely match patients' bone defects (Lee et al., 2013; Yao et al., 2015; Temple et al., 2014; Xu et al., 2014).

A variety of AM techniques including 3DP, stereolithography (SLA), fused deposition modeling (FDM), and selective laser sintering (SLS) have been developed for tissue engineering applications (Lee et al., 2010; Butscher et al., 2011; Bose et al., 2013; Kumar et al., 2016b).

Powder-based 3D printing is considered a particularly promising bone reconstruction technique as the external shape, internal structure, porosity, and material properties of 3D printed bone substitutes can be varied and thus prepared for specific applications. Synthetic bone substitutes, in particular calcium phosphate (CaP) powder, which can be used to generate 3D printed bone scaffolds (Butscher et al., 2013; Castilho et al., 2014a), are considered particularly interesting solutions for bone tissue repair (Habibovic et al., 2008; Tamimi et al., 2008).

A recent promising approach consists in combining growth factors (GFs) or drugs with osteoconductive scaffolds. This strategy promotes a faster and more significant enhancement of new bone formation thanks to GF or drug delivery and because of the tridimensional stability of the scaffold, which provides protection during the gradual replacement of the graft with newly-formed bone. Various materials have been used to this aim, including inorganic bovine bone, porous hydroxyapatite, and demineralized human bone matrix (Sivolella et al., 2013). Calcium phosphates 3D printed scaffolds have also been used for growth factor and drug delivery (Bose et al., 2013).

This article intends to outline the main features of the most common AM technologies (3D printing, stereolithography, fused deposition modeling, and selective laser sintering) used to fabricate porous scaffolds for bone tissue engineering; it will go on to give a brief overview of 3D printing technology, including a description of the properties of powders and binder solutions, the critical phases of scaffold manufacturing, and its applications in tissue engineering. It also addresses current limitations of a technology which should ideally be site-specific. Clinical aspects and future applications of powder-based 3D printed constructs in bone tissue engineering are also discussed.

2. Material and methods

A Medline (PubMed) search was performed in duplicate for studies regarding the application of powder-based three-dimensional printing (3DP) for the production of bone tissue engineering scaffolds. The Medical Subject Heading (Mesh) term “three-dimensional printing” was used together with the term “bone” applying the following search strategy: ((“printing, three-dimensional”[MeSH Terms] OR (“printing”[All Fields] AND “three-dimensional”[All Fields]) OR “three-dimensional printing”[All Fields] OR (“three”[All Fields] AND “dimensional”[All Fields] AND “printing”[All Fields]) OR “three dimensional printing”[All Fields]) AND (“bone and bones”[MeSH Terms] OR (“bone”[All Fields] AND “bones”[All Fields]) OR “bone and bones”[All Fields] OR “bone”[All Fields])) AND (“2010/01/01”[PDAT]: “2016/02/29”[PDAT]).

The on-line database was searched to find articles published in the English language between January 1st 2010 until February 29th 2016. All *in vitro*, *in vivo*, and human studies regarding the use of powder-based 3DP printing for the synthesis of bone tissue engineering scaffolds were considered. No limitations with regard to sample size or length of follow-up period were applied.

Systematic reviews and meta analyses were not considered. Studies dealing with the following topics were excluded: 3D printed templates for dental implant positioning or osteotomy design, 3D printed anatomic templates for preoperative planning or training.

2.1. Study selection

The titles and abstracts, whenever available, that were identified by the electronic search were independently screened by two of the authors, and any disagreements were resolved by a discussion between them. Full-text articles of studies appearing to meet the inclusion criteria or in those cases in which the title and/or abstract did not provide sufficient data were requested from their authors. The studies that were selected were then screened independently by both of the reviewers, and disagreements were resolved by discussion.

2.2. Data extraction

Two of the authors independently extracted and analyzed the data, and the consensus of the other authors was sought at this point of the process.

The following data were registered: the authors' names, the year of publication, the material used to produce the scaffolds, the main features of the scaffold structure, and the production steps.

3. Results

3.1. Additive manufacturing (AM) technologies

Several additive manufacturing (AM) technologies have been developed to produce 3D porous interconnected scaffolds using computer aided design (CAD) software allowing good control of their internal and external architecture. These technologies have provided innovative methods for successful patient-specific bone tissue engineering applications. Based on multi-layered 3D structures, all AM techniques can be used to manufacture precise, predefined scaffolds directly from CAD data without any need for an intermediate molding passage. The process consists in converting CAD data into multiple 2D cross-sectional layers; the 3D printer then creates the target structure following the pre-defined 2D pattern. A brief overview of the most important AM techniques including 3D printing (3DP), stereolithography (SLA), fused deposition modeling (FDM), and selective laser sintering (SLS) is presented below.

3.1.1. 3D printing

With a high application potential for bone tissue engineering and considered one of the most attractive AM systems, 3DP technology was developed at the Massachusetts Institute of Technology in 1995 (Lee et al., 2010).

A first layer of powder is laid on the building platform, and, following the pattern of the 2D image of the first cross-section, a liquid binder is sprayed on the surface of the powder layer bonding together the powder granules. Once the layer is completed, the platform is lowered the height of one layer and a new one is laid over the precedent one. This process is repeated until all of the layers have been printed. The structure is supported throughout the process by the surrounding unprocessed powder (Fig. 1). The printed structure, embedded in the loose powder, must be extracted from the powder bed after it has been printed, and the unbound powder must be removed from its pores and cavities, a crucial step in the printing process that is referred to as depowdering. The scaffold can then be sintered (Seitz et al., 2005; Lee et al., 2010).

Powder solidification is not achieved by means of polymeric gluing in low temperature 3D printing but *via* a hydraulic setting reaction (Castilho et al., 2014b; Gbureck et al., 2007a). Requiring no further thermal treatment, the method enables the incorporation of bioactive molecules and drugs during the 3D printing process (Vorndran et al., 2010).

3D printing can be adapted to produce porous ceramic-based bone scaffolds with well defined inner and external structures for bone tissue engineering (Warnke et al., 2010). As the validity of this method has also been demonstrated *in vivo* (Tamimi et al., 2014; Torres et al., 2011; Castilho et al., 2014b), many investigators are convinced that it will find a number of applications in the near future in clinical practice.

Some authors have presented an alternative to 3D printing, called indirect 3DP (Lee et al., 2005, 2013; Tamjid et al., 2013); in this case a positive replica of a predetermined shape is printed, and a biodegradable polymer solution is cast into a printed mold cavity. While the approach overcomes one of the major drawbacks of 3DP, which consists in the undesirable use of common synthetic biodegradable polymers since organic solvents as binders can dissolve most commercial printheads (Lee et al., 2013; Chia and Wu, 2015), it is unable to produce scaffolds with well-defined complex internal architectures because of the difficulty in removing the plaster mold from the internal pores (Lee et al., 2013; Tamjid et al., 2013).

3.1.2. Stereolithography

Although independently, Kodama (1981) and Nakai and Marutani, (1986) introduced and developed stereolithography at the same time (in the '80s). The technique consists in exposing a liquid photo-hardening polymer to ultraviolet rays and stacking the cross-sectional solidified layers. An ultraviolet laser beam selectively irradiates the surface of the liquid photo-polymer and hardens it. The solidified layers are overlapped, and a cross-sectional structure is generated (Kodama, 1981). In the 1990s, Ikuta et al. (1994) developed microstereolithography (MSTL), a precise technique enabling much higher spatial resolution that is capable of solidifying smaller areas of a photopolymer using a focusing lens.

Many biomaterials with good photo-polymerization capabilities such as polypropylene fumarate (PPF)-based materials, gelatin-based materials, and trimethylene carbonate (TMC)-based materials have been actively studied in recent years for bone tissue engineering applications (Lee et al., 2010).

SLA's major limitation is that it uses photocurable resins, which typically lack the approval of the U.S. Food and Drug Administration (Korpela et al., 2013; Chia and Wu, 2015), as printing materials.

3.1.3. Fused deposition modeling

Fused deposition modeling is an AM technique that utilizes thermoplastic fiber that is heated and selectively extruded out of nozzles moving within the x- and y-axes layer-by-layer. The semi-molden polymer is extruded onto a base plate following a path predetermined by CAD specifications. When a layer is completed, the base platform is lowered vertically on the *z*-axis and another layer of thermoplastic polymer is delivered. This process is repeated until the structure has been completed (Lee et al., 2010; Korpela et al., 2013; Meakin et al., 2004). Several biodegradable materials have been used in the process, in particular polycaprolactone (PCL) (Hutmacher et al., 2001) whose inherent low strength and slow degradation rate limit its bone tissue engineering applications (Idaszek et al., 2015). Other polymers used in FDM processes are poly(D,L-lactide-coglycolide) (PLGA) (Yen et al., 2009) and poly(D,L-lactide) (PDL) (Hsu et al., 2007). Some composites such as PCL/tricalciumphosphate (TCP) (Teo et al., 2011), PLGA/TCP/hydroxyapatite (HA) (Kim et al., 2012), and PCL/PLGA/TCP (Kim et al., 2010) have also been investigated. CT-guided FDM has also been used to fabricate PCL/HA artificial grafts to mimic natural goat femurs, and the performance of artificial bones in a long load-bearing goat femur bone segmental defect model was found to be good (Xu et al., 2014).

3.1.4. Selective laser sintering

Developed at the end of the '80s at the University of Texas, selective laser sintering is an AM technique that uses a high-power laser to melt thin layers of powder for structure production. The laser beam selectively fuses powders following the cross-sectional information carried by the CAD data. During sintering, the laser beam-powder interaction increases the temperature inducing fusion of adjacent particles. After a layer is created, the powder bed is lowered and another layer of powder is rolled over it; the process is repeated layer after layer until the scaffold is completed. Unlike what happens with SLA, temporary support structures are not needed during the process, as support is provided by the unbound powder and, just as in 3DP, all remaining powder is removed after the scaffold has been completed (Chia and Wu, 2015; Lee et al., 2010).

SLS can create complex structures, including bone tissue engineering scaffolds, from a relatively wide range of powder materials such as poly(lactic acid), PCL and bio-ceramics. Hydroxyapatite (HA), for example, has been blended with PCL (Wiria et al., 2007), and *in vitro* cell ingrowth into scaffolds has been reported. There have also been reports on scaffolds processed *via in vivo* laser sintering. Both nano-HA/PCL

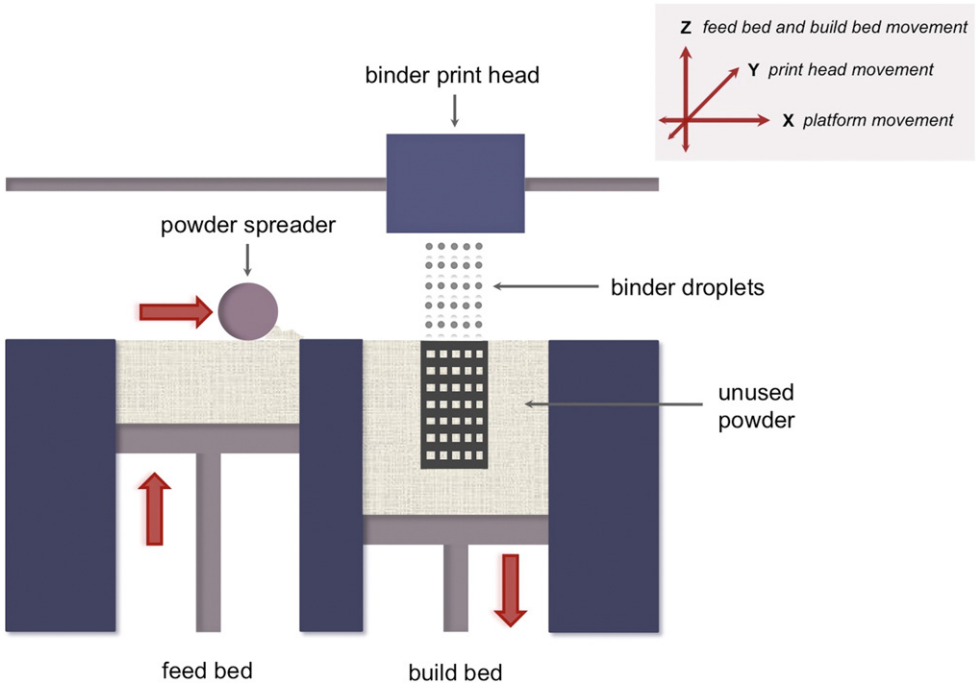

Fig. 1. Schematic drawing representing the 3D printing process. Figure from Bose et al. (2013) modified.

and PCL scaffolds produced using SLS techniques were implanted in rabbit femur defects; the results showed good biocompatibility and promotion of healing of bone defects (Xia et al., 2013).

Although the potential of scaffolds fabricated *via* SLS for bone tissue engineering has been recognized, the technique does present some limitations given the high operating temperatures needed during the manufacturing process (Chia and Wu, 2015).

3.2. Powder-based 3D printing

Powder-based 3D printing is characterized by various features (*i.e.* powders and binders, depowdering, post-processing treatments, sintering, mechanical properties, scaffold customization) which are presented in detail in the following paragraphs and summarized in Table 1.

3.2.1. Powders and binders

Various powders that can be selectively solidified by different binders sprayed onto powder layers during the process can be used in 3DP for bone tissue engineering.

Calcium phosphate (CaP) bioceramics, which exhibit excellent osteoconductive properties due to their chemical similarity to natural bone, are widely used to fabricate porous scaffolds for bone tissue engineering applications, (Woodard et al., 2007; Detsch et al., 2008; Raynaud et al., 2002).

Alpha-tricalcium phosphate (TCP) powders are usually printed using diluted phosphoric acid as the binder solution for synthetic graft production (Torres et al., 2011; Tamimi et al., 2014; Klammert et al., 2010a; Castilho et al., 2013, 2014a).

In vitro studies have been performed to assess osteoblast cell proliferation on sintered 3D printed interconnected macroporous β-TCP scaffolds with different pore sizes (Tarafder et al., 2013a) (Fig. 2). The fact that all the samples that have been produced using β-TCP and a solvent based binder showed good cell proliferation and ingrowth into porous structures has confirmed the biocompatibility of the materials utilized. An increase in cell density with a decrease in macropore size has nevertheless been reported.

TCP properties can be improved and modified by adding additional dopants such as SrO and MgO (Tarafder et al., 2013b, 2015) or SiO_2 and ZnO (Fielding and Bose, 2013) to the powder.

Just as CaP, HA is a material that is widely used in 3D printed artificial bone scaffold fabrication (Wang et al., 2014, 2015; Detsch et al., 2011; Warnke et al., 2010).

An *in vitro* study examining the biocompatibility of 3D printed HA and TCP sintered scaffolds was performed using human osteoblasts (Warnke et al., 2010). While both samples were colonized by cells showing a well-spread morphology at Scanning Electron Microscope (SEM) investigations 7 days after seeding, cell vitality staining and MTT, LDH, and WST tests identified superior biocompatibility of the HA scaffolds with respect to the TCP ones.

α-*n*-butyl cyanoacrylate (NBCA) was investigated as a liquid binder sprayed on the surface of an HA powder layer. Bone scaffolds of different strengths can be fabricated by controlling and adjusting the doses of the binder sprayed on the powder layers during the 3D printing process (Wang et al., 2014, 2015).

Biphasic calcium phosphate (BCP) ceramics consist in different HA and beta-tricalcium phosphate (β-TCP) mixtures. The combination of β-TCP reactivity and HA stability improves bioactivity while retaining degradability (Hutmacher et al., 2007). The dissolution rate of the biphasic mixture can be varied by mixing various proportions of the more soluble β-TCP with HA (LeGeros et al., 2003). The scaffolds' degradation takes place not only through solubility but also by osteoblast resorption. As demonstrated by lacunae formation on scaffold surfaces after 21 days in culture (Detsch et al., 2011), sintered BCP scaffolds produced using 3DP technology seem better able to activate osteoclasts with respect to HA and β-TCP.

BCP scaffolds also showed good cytocompatibility during an *in vitro* study conducted by Castilho et al. (2014a) who reported significantly higher osteoblastic cell viability and cell proliferation levels in BCP printed scaffolds with respect to those in pure TCP scaffolds.

As far as biphasic calcium phosphate scaffolds produced using a 3D printing method are concerned, Rath et al. (2012) and Strobel et al. (2014) proposed a different method that combines 3DP technology with the salt leaching process based on space-filling agents. This novel method is based on 3DP printing of biomaterials such as biphasic CaP

along with starch, a pore-forming agent. The water-glycerol binder solution causes the dextrin granules to burst, and sintering of the embedded starch leads to the generation of void spaces within the scaffold.

Rath et al. (2012) performed preliminary *in vitro* tests to evaluate the effect of dynamic with respect to static 3D culture conditions when osteogenic cells (osteoblasts and bone marrow derived stromal cells) are seeded on 3D printed biphasic CaP scaffolds under basal and osteoinductive culture conditions. The scaffold that was produced had a compressive strength of 3.5 MPa, which is considered in the normal for cancellous bone (Athanasiou et al., 2000), and a laminar medium flow through the porous BCP scaffolds in the bioreactor perfusion system was thus ensured. As the dynamic culture conditions improved the survival rate and ostegenic differentiation of the seeded cells on the scaffold under dexamethasone-mediated osteoinduction, their future application in the *in vitro* generation of cell-loaded 3D constructs has been implied.

Strobel et al. (2014) did not, however, confirm those results in a subcutaneous rat model when scaffolds pre-cultivated in a perfusion flow bioreactor for six weeks were compared to those freshly seeded before they were implanted subcutaneously. Dynamic culture conditions did not additionally enhance the osteogenic properties in the *in vivo* experimental setting.

While many attempts have been made to fabricate CaP-based scaffolds, the setting reaction of acid binders that these materials usually requires continues to pose major concerns. The use of an acid binder, such as phosphoric acid, significantly compromises printhead performance (Rahmati et al., 2009; Zhou et al., 2014), and removing the toxic solvents at the end of the printing process continues to be a problem (Detsch et al., 2011).

To overcome the limitations linked to acidic binders, Zhou et al. (2014) proposed blending CaP powder with a biocompatible, biodegradable calcium sulfate ($CaSO_4$)-based powder additive to enable a reaction with a water-based binder thus eliminating the requirement of an acidic binder. The authors reported that HA:$CaSO_4$ scaffolds had higher wetting ratios and green strength with respect to scaffolds printed using β-TCP:$CaSO_4$ powder combinations.

Given its low strength and rapid resorption rate, $CaSO_4$ alone has been gradually substituted by CaP-based composites. Plaster has excellent printability in thermal ink-jet 3DP manufacturing and enables a reaction with a water-based medium (Farzadi et al., 2014). Just as Zhou et al. (2014) reported, $CaSO_4$ eliminates any need for an acidic binder or water solution suspended with polyvinyl materials that increases the nozzle wear rate and the degradation of heating elements in the thermal print head. Mixing $CaSO_4$-based powders with water activates a self-hydration reaction that leads to recrystallization into a solid form of gypsum.

Poly(vinyl)alcohol (PVOH) composite powders were instead used by Cox et al. (2015) who selected a partially hydrolysed grade of PVOH to enable dissolution when wetted with a water-based binder during printing.

Polymeric binders are removed during sintering by pyrolysis. *In vitro* tests have confirmed good biocompatibility of CaP ceramics. All organic additives are thus burned out during the sintering process leaving no toxic residues (Detsch et al., 2011).

Green bodies do not need to undergo the sintering process in low temperature 3D printing. Some investigators have proposed elevating the samples to remove the residual acidity of the acid binder solution (Klammert et al., 2009). Inzana et al. (2014) avoided the thorough rinsing technique and considered the possibility of eluting any bioactive molecules that were printed into the constructs. They achieved an optimal balance between cytocompatibility and material strength by using 8.75 wt.% phosphoric acid as the binder solution.

Magnesium ammonium phosphate (struvite) structures have also been obtained with low temperature 3D printing. Acid binding was avoided by printing farringtonite powder with ammonium phosphate solution as a binder in a neutral setting reaction (Klammert et al., 2010b).

3.2.2. Depowdering

Depowdering, which consists in removing the unglued granules from the pore structure after printing, is a post-processing step. The scaffold (green body) produced is extracted from the building platform, and the loosely adhering powder is removed *via* air blowing and/or dry ultrasonication (Detsch et al., 2011; Tarafder et al., 2013b; Castilho et al., 2014b).

Using compressed air to remove the loose powder can damage those green structures that are mechanically unsuitable for safe handling and depowering. Cox et al. (2015) printed scaffolds from HA:PVOH precursors in ratios ranging between 0:100 and 100:0 wt.%. Only scaffolds produced from 50 and 60 wt.% HA had stable green bodies. Indeed, structures produced from a 60:40 HA to PVOH ratio resulted quite difficult to handle and was easily damaged during this step due to weak bonding between layers. No apparent damage or de-bonding of layers occurred during depowdering of 50 wt.% HA green scaffolds deemed mechanically suitable and stable.

Depowdering is considered critical in direct 3DP processes not only for green structure stability but also for complex interconnected porous architectures. Controlling pore size and porosity in the middle of large scaffolds continues to remain a challenging task.

Butscher et al. (2013) proposed a new approach to overcome the difficulty of removing loose powder from printed scaffolds and investigated CaP scaffolds with complex shapes and structures. Those investigators quantified depowdering efficiency by calculating the solid volume fraction (BV/TV) of the samples from μCT data. The best results were obtained for those scaffolds whose free fillers had great distances between one another. The structures were composed for the most part of convex fillers caught in an outer cage whose windows were large enough to enable depowdering but were still able to trap loose fillers placed inside the cage. Although the free fillers presented excellent depowdering characteristics, movement between the fillers was limited and this may have a negative effect on bone remodeling. A post-hardening process could be applied to stabilize and interlock the fillers.

The influence of layer thickness and printing orientations (parallel to the X, Y and Z directions) on depowdering is also critical. Farzadi et al. (2014) produced scaffolds whose pore sizes were 0.4, 0.6, and 0.8 mm. Depowdering the samples with 0.4 and 0.6 mm pore sizes could not be accomplished corrrectly and those samples had deteriorated structures after printing. Only the scaffolds having a 0.8 mm pore size printed with different layer thicknesses and printing orientations were thus considered for further characterization. The samples printed in the X direction were slightly depowered compared to those printed in the Y direction. A longer average time was, moreover, necessary to completely depowder the samples printed in the Z direction. It was more difficult to depowder the initial surface to be printed in all the samples and it took longer with respect to the time necessary for the other sides. As in a previous study (Butscher et al., 2013), the depowdering efficiency was calculated on the basis of μCT data. The theoretical values based on CAD models were compared with the corresponding BV/TV measured values. The samples with 0.1125 mm layer thickness printed in the X direction had porosity and pore volume values that were the most similar to CAD designed values and this confirmed that they had undergone a thorough depowdering.

The mechanical stability of green bodies is fundamental in preventing shape changes or, ultimately, mechanical failure during depowdering. Even the weight of unbound powder may be critical for weak scaffold structures (Butscher et al., 2011; Lee et al., 1995). Butscher et al. (2013) found sufficient mechanical stability of green bodies, even for samples with free fillers inside, as damage of filigree design features was not caused during depowdering.

Scaffold fabrication using 3DP technologies must still undergo the depowdering step, and this remains a major challenge as far as the

Table 1
Summary of powder-based 3D printing main features.

Powder	Binder	Layer thickness [μm]	Binder/volume ratio and/or saturation (%)	Depowdering	Post-processing	Sintering	Further treatments	References
HA	α-n-butyl cyanoacrylate (NBCA)	–	–	–	–	–	–	Wang et al. (2015)
HA/PVOH (various ratios, from 0:100 to 100:0 wt.%)	Water based binder	100 μm	Maximum binder saturation level	Compressed air	– Left as printed – Furnace dried 2 h – Vacuum dried 2 h – Furnace dried 6 h – Vacuum dried 6 h	– No sintering – Sintered using a two-step Heating protocol: (1) 30–230 °C at 0.5 °C/min, and (2) 230–1300 °C at 2 °C/min. Constructs were held at 1300 °C for 1 h and then cooled to 30 °C at 2 °C/min.	–	Cox et al. (2015)
Calcium sulfate based powder (zp150)	Water based solution with 2-Pyrrolidone (zb6)	87.5 μm 100 μm 112.5 μm 125 μm	0.24 (shell) and 0.12 (core); saturation 100%	Compressed air	–	–	–	Farzadi et al. (2014)
– β-TCP – SrO-Mg-doped β-TCP	solvent based binder	20 μm	–	Dry ultrasonication and/or air blowing	Hardened at 175 °C for 90 min	– Sintered at 1250 °C in conventional muffle Furnace for 2 h – Sintered at 1250 °C in microwave furnace for 1 h	–	Tarafder et al. (2015)
– β-TCP – SrO-Mg-doped β-TCP	Solvent based binder	20 μm	–	Dry ultrasonication and/or air blowing	Hardened at 175 °C for 90 min	Sintered at 1250 °C in microwave furnace for 1 h	–	Tarafder et al. (2013b)
β-TCP	20% phosphoric acid	–	–	Unspecified	Stored in 20% phosphoric acid 3 × 60 s	–	Dehydrated into monetite and sterilized by autoclaving (121 °C; humidity 100%; 30 min)	Tamimi et al. (2014)
TCP	20% (v/v) phosphoric acid	125 μm	0.26	Compressed air	Post-hardened by immersion in binder solution for 30 s following drying in air			Castilho et al. (2014b)
– HA:$CaSO_4$ (25:75 wt.%) – HA:$CaSO_4$ (50:50 wt.%) – β-TCP:$CaSO_4$ (25:75 wt.%) – β-TCP:$CaSO_4$ (50:50 wt.%)	Water based binder	–	–	Compressed air	–	–	–	Zhou et al. (2014)
HA/α-TCP	– 8.75 wt.% phosphoric acid + 0.25 wt.% Tween 80 – 8.75 wt.% phosphoric acid + 0.25 wt.% Tween 80 + 1 wt.% collagen – (12.5 wt.% phosphoric acid) – (8.75 wt.% phosphoric acid) – (5% wt.% phosphoric acid)	89 μm	0.46	Unspecified	Post-processed by flash dipping in 0.1 wt.% phosphoric acid and then washing in deionized water (3 × 120 s)	–	– No treatment – Coated with a 0.5 wt% neutralized collagen gel (only some samples obtain with binder: 8.75 wt% phosphoric acid + 0.25 wt% Tween 80)	Inzana et al. (2014)
ZP113	ZB-58	–	–	Unspecified	Infiltrated using epoxy ZMax resin and left overnight to dry	–	–	Lipowiecki et al. (2014)
TCP and calcium carbonate	10% (v/v) phosphoric acid	112 μm	0.30	Unspecified	–	Sintered at 1200 °C for 5, 10 or 15 h with a heating rate of 1° min^{-1}	– No treatment – immersed In PBS for 6 days	Castilho et al.

(continued on next page)

Table 1 (*continued*)

Powder	Binder	Layer thickness [μm]	Binder/volume ratio and/or saturation (%)	Depowdering	Post-processing	Sintering	Further treatments	References
							– Immersed in PBS for 6 days, followed by drying in air and immersing each sample in 10 wt.% 75/25 PLGA-solution	(2014a)
HA	α-n-butyl cyanoacrylate (NBCA)	–	–	–	–	–	–	Wang et al. (2014)
α-TCP	10 wt.% phosphoric acid	50 μm	Saturation: 45% for the shell; 90% for the core	Airstream	– No post-hardening – Post-hardening: full dip in 10 wt.% phosphoric acid (~5 s) – Post-hardening: partial dip in 10 wt.% phosphoric acid (~5 s)	–	–	Butscher et al. (2013)
TCP	20% (v/v) phosphoric acid	125 μm	0.26	Unspecified	Posthardened in the binder solution for 1 × 30 s	–	–	Castilho et al. (2013)
– β-TCP – SiO_2-ZnO-doped β-TCP	Water based binder	– 20 μm (β-TCP) – 30 μm (SiO_2-ZnO-doped β-TCP)	– 110% saturation (β-TCP) – 100% saturation (SiO_2-ZnO-doped β-TCP)	Gently brushed clean, compressed air blower	–	Sintered in a muffle furnace at 1250 °C for 2 h	Autoclaving at 121 °C for 20 min	Fielding and Bose (2013)
HA (35 wt%) – β-TCP (35 wt.%) – acid-hydrolytic modified potato starch powder (dextrin) (30 wt.%)	Water-glycerol (15 wt.%)	100 μm	–	–	POST-heating 2 h at 75 °C; subsequent heating to 120 °C with a heating rate of 5.5 °C/min; further heating to 350 °C followed by a dwell period of 1 h at 350 °C	Sintered at 1200 °C for 4 h	Grinded with 80 mm grit *SiC* sandpaper	Strobel et al. (2014)
β-TCP	Aqueous based binder	20 μm	110% saturation	Dry ultrasonication and/or air blowing	Hardened at 175 °C for 90 min	– Sintered at 1150 °C in conventional muffle furnace for 2 h – Sintered at 1250 °C in conventional muffle furnace for 2 h – Sintered at 1150 °C in microwave furnace for 1 h – Sintered at 1250 °C in microwave furnace for 1 h	–	Tarafder et al. (2013a)
HA (35 wt.%) – β-TCP (35 wt%) – acid-hydrolytic modified potato starch powder (dextrin) (30 wt.%)	–	–	–	–	–	Sintered at 1200 °C in electrically headed furnace	Sterilized in 70% ethanol + UV light illumination; coated with 0.01% collagen and washed in culture media before seeding	Rath et al. (2012)
β-TCP	Phosphoric acid (20% wt)	–	–	Unspecified	Stored in phosphoric acid (20% wt.) 3 × 60 s	–	Dehydrated into monetite and sterilized by autoclaving (121 °C; humidity 100%; 30 min)	Torres et al. (2011)
– Farringtonite – Farringtonite modified with 20% diammonium hydrogen phosphate (DAHP)	0.75 M diammonium hydrogen phosphate + 0.75 ammonium dihydrogen phosphate	125 μm	0.371	Unspecified	Post-hardened by immersion in the binder solution for 24 h. Finally, the scaffolds were rinsed 3 times with distilled water, soaked with 70% ethanol and air-dried.	–	–	Klammert et al. (2010b)
– HA – β-TCP – HA/β-TCP 60/40 wt% (BCP sample)	Unspecified	100 μm	–	Air blower	–	Sintered at 1300 °C in an electrically heated chamber furnace in air for 1 h	–	Detsch et al. (2011)
– TCP (45% α-TCP; 55% β-TCP)	Phosphoric acid (20% wt)	–	–	Unspecified	Post-hardened by immersion in 20 wt% phosphoric acid for 2 × 30 s	–	Autoclaving at 134 °C for 2 h	Klammert et al. (2010a)
– HA – TCP	Polymeric binder Schelofix [dissolved in water 10 and 14 wt.%]	[200 μm; 250 μm; 300 μm]	–	Air blower	–	Sintered at 1250 °C for 2 h in an electrically heated chamber furnace in ambient air	–	Warnke et al. (2010)

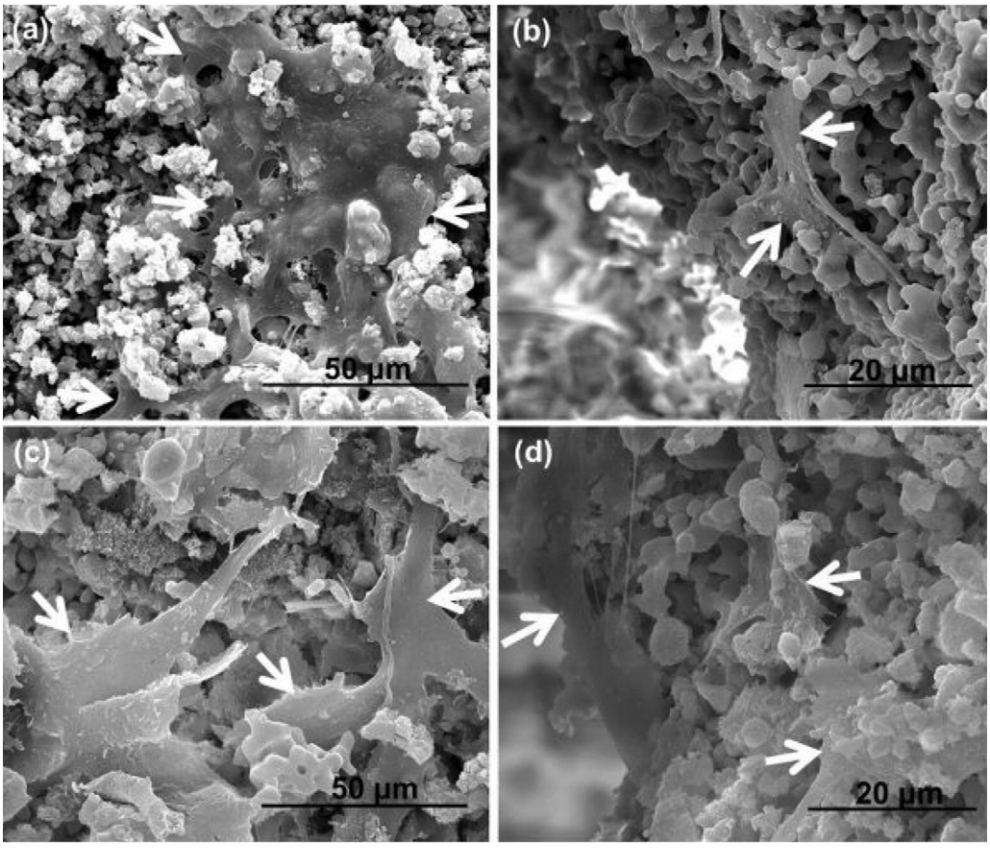

Fig. 2. SEM micrographs of human fetal osteoblast (hFOB) cells showing the cell adhesion and proliferation on and inside themicrowave sintered 3D printed interconnected macro porous TCP scaffold after 3 days of culture (white arrows indicate cells): 500 μm (a) & (b), and 750 μm (c) & (d). Figure from Tarafder et al. (2013a).

production of complex interconnected pore structures is concerned. Serious efforts aiming to improve depowdering efficiency, in particular for scaffolds of large dimensions or with complex internal architectures, must continue to be made.

3.2.3. Post-processing treatments, sintering, mechanical properties

Green strength refers to the initial strength of a scaffold after printing but before any post-processing phases are carried out to increase mechanical properties. This property is of primary importance in printed scaffolds because low green strength may lead to shape changes or damage to the green bodies when they are retrieved from the powder bed and depowered (Cox et al., 2015; Butscher et al., 2011).

Green strength is primarily conditioned by pore size, porosity, and pore distribution. Although, generally speaking, an apparently higher density results in better mechanical properties (Gbureck et al., 2007a; Butscher et al., 2011), a more pronounced vascularization is achieved when scaffolds are more porous, and therefore weaker (Will et al., 2008). Higher permeability values have been registered for scaffolds with greater porosity and mean pore sizes (Lipowiecki et al., 2014). Porous 3D printed CaP structures favour bone infiltration within the scaffold and nutrient delivery and facilitate mechanical interlocking between the scaffolds and the recipient site. It is critically important to fabricate 3D printed scaffolds with large voids for high-load bearing applications in bone tissue regeneration (Farzadi et al., 2015; Zhou et al., 2014).

Porous scaffolds usually need to be post-processed after printing, by dipping them in a binder solution (Castilho et al., 2014b; Inzana et al., 2014; Torres et al., 2011) or by sintering (Tarafder et al., 2013b, 2015; Cox et al., 2015) (Fig. 3), to enhance their mechanical properties.

Butscher et al. (2013) who post-hardened printed CaP scaffolds achieved improved mechanical properties. The post-processing treatment, consisting in the full or partial immersion of samples into phosphoric acid, decreased the porosity and the α-TCP content and increased the reaction of TCP into brushite and monetite. This explains the higher compressive and diametral tensile strengths of cylindrical post-hardened scaffolds following both types of dipping methods (full or partial) with respect to the values of printed green bodies.

Cox et al. (2015) fabricated porous 3D printed scaffolds from HA and poly(vinyl)alcohol composite powder. Post-processing of the samples, consisting in drying the green scaffolds in a furnace or in a vacuum oven, led to a reduction in the constructs' average height, diameter, and weight. The structure's higher degree of consolidation during the post-processing treatment may explain the higher yield and the ultimate compressive strength of the dried samples.

Greater strength can be achieved by sintering the scaffolds, and production of 3D printed ceramic scaffolds often, in fact, involves sintering. Sintering of ceramics has widely been used to improve the mechanical properties of scaffolds produced for bone tissue engineering applications. CaP powder is bound by a polymeric glue to form a green body which is then sintered (Seitz et al., 2005). As sintering leads to specimen shrinkage, this must be taken into consideration during the CAD phase. Changes in dimensions must be precalculated by CAD which designs custom-made site-specific bone graft substitutes (Fielding and Bose, 2013; Warnke et al., 2010; Seitz et al., 2005; Castilho et al., 2014a; Cox et al., 2015).

While sintered biphasic CaP scaffolds with a *Ca*/P ratio of 1.83 produced different ultimate compressive strengths and toughnesses depending on post-treatments (Castilho et al., 2014a), immerging the scaffolds in PBS had no significant effect on the specimens' mechanical

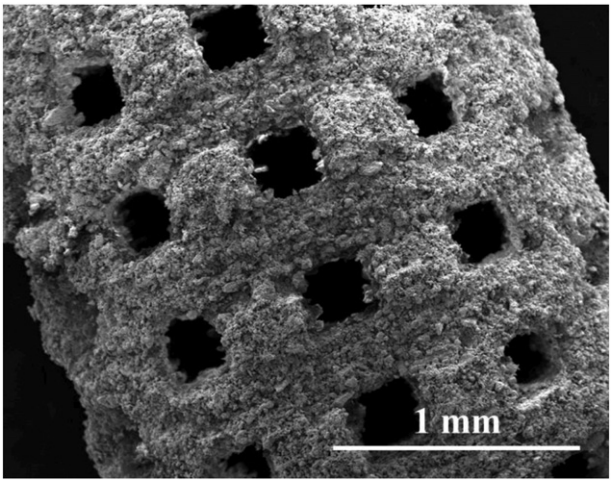

Fig. 3. SEM image of microwave sintered pure TCP scaffold. Figure from Tarafder et al. (2013b).

properties. Post-treatment of the sintered scaffolds with a polylactic-*co*-glycolicacid (PLGA)-solution was found to enhance their compressive strength by a factor of 8, regardless of prior PBS immersion, and their modulus of toughness by a factor of 4.

Other authors (Rath et al., 2012; Strobel et al., 2014) described a method consisting in 3D printing of biphasic CaP scaffolds together with a pore-forming agent, dextrin, followed by sintering the constructs progressively until 1200 °C was reached in an electrically heated furnace. Heating the embedded starch generated void spaces within these highly interconnected porous scaffolds. This method can be used to (Rath et al., 2012; Strobel et al., 2014) produce custom-made individualized scaffolds with shapes and properties tailored to the specific critical-size bone defect, modify the HA/β-TCP ratio and starch compound and create porosity gradients and local structural reinforcements.

Another promising method is based on microwave heating of sintered samples. When a construct is sintered in a conventional electric muffle furnace, the heat dissipates inward into the object through radiation, conduction and convection. Unlike what occurs during conventional sintering, the construct itself absorbs the microwave energy as electric-

magnetic radiation and transforms it into heat within the sample volume (Yadoji et al., 2003). Some of the advantages of microwave processing are improved heating uniformity, enhanced reactions and sintering rates, and reduced processing times, all leading to controlled grain growth, higher densification and, ultimately, improved mechanical properties (Yadoji et al., 2003; Bose et al., 2010).

The advantages of microwave processing of ceramics over conventional sintering have been described by Tarafder et al. (2013a). Microwave sintered β-TCP scaffolds were found to have higher mechanical properties with respect to samples sintered in conventional electric furnaces. Microwave sintered scaffolds resulted in higher densification and shrinkage, leading to a decrease in pore size. When the sintering temperature is increased (from 1150 °C to 1250 °C) the total porosity is decreased. A more uniform shrinkage along different directions of the scaffolds has been observed in microwave sintered samples. The superior densification and shrinkage of microwave sintered scaffolds contribute to their higher compressive strength with respect to conventionally sintered samples. A maximum compressive strength (10.95 ± 1.28 MPa) has been obtained by scaffolds with 500 μm macropores and 42% total volume fraction porosity when sintered at a higher temperature (1250 °C for 1 h) in a microwave furnace.

Tarafder et al. (2013b) compared the values of microwave sintered pure TCP scaffolds with results outlined in a previous work (Tarafder et al., 2013a) focusing on SrO-MgO doped TCP scaffolds. A maximum compressive strength value of 12.01 ± 1.56 MPa was achieved for 500 μm interconnected designed pore size SrO–MgO doped scaffolds. The additional SrO–MgO dopants in the β-TCP powder affected its phase stability. Microwave processing at 1250° resulted in β- to less dense α-TCP transformation, which negatively influenced the scaffolds' mechanical properties due to spontaneous microcrack development (Tarafder et al., 2013a). Unlike pure TCP, the absence of α-TCP formation was detected at 1250 °C sintering temperature in SrO-MgO doped TCP, indicating high-temperature phase stability that can probably be explained by the presence of Mg^{2+} (Tarafder et al., 2013b).

Tarafder et al. (2015) recently evaluated the influence of sintering on the mechanical properties of SrO–MgO doped 3D printed TCP scaffolds with different interconnected pore sizes. The samples were sintered at 1250 °C in a conventional muffle furnace for 2 h or in a microwave furnace for 1 h. Microwave processing enhanced the densification of the doped TCP scaffold with respect to conventional sintering. SrO–MgO doped samples did not uncover any α-TCP peaks for either sintering methods, meaning that there was no β to α phase high temperature transformation. Microwave processing contributed to a reduction in the grain size of TCP scaffolds. An increase in compressive strength linked to microwave sintering and a decrease in pore size was noted.

Adding SrO–MgO dopants in β-TCP and microwave sintering enhanced the mechanical properties of these 3D printed macroporous TCP scaffolds (Tarafder et al., 2013a, 2013b, 2015).

Other dopants can also be successfully used as sintering additives in TCP ceramic scaffolds to reduce the transformation of β-TCP to α-TCP at temperatures above 1150 °C. Fielding et al. (2012) demonstrated that α-TCP phase formation was reduced in silica (SiO_2) and zinc oxide (ZnO) doped samples with respect to pure TCP scaffolds after conventional sintering at 1250 °C. Doped samples presented higher densification and showed up to a 250% increase in compressive strength compared to that in pure TCP scaffolds; when those scaffolds were used in a murine femoral defect model, they had a positive influence on neovascularization and new bone formation (Fielding and Bose, 2013) (Fig. 4).

In an approach proposed by Gbureck et al. (2007a) and referred to as low temperature 3D printing, a binder reacts with CaP powder particles in an hydraulic setting reaction forming a stiff ceramic network. The main advantage of this technique is linked to the possibility of incorporating heat-labile bioactive molecules and drugs during the 3D printing process.

Successful production of tailored CaP bone substitutes was achieved by low temperature 3D printing using diluted phosphoric acid and β-TCP powder (Gbureck et al., 2007a). This process leads to the formation of dicalcium phosphate dehydrate (brushite) scaffolds, which can be further modified by hydrothermal treatment using an autoclave, causing the conversion of brushite into dicalcium phosphate anhydrous (monetite). These are, in fact, sterilizable by gamma irradiation (Castilho et al., 2014b) or autoclaving (Klammert et al., 2010a), the latter leading to monetite due to the hydrothermal conversion of brushite.

In vivo performances of these low temperature 3D printed scaffolds have been assessed in ectopic models of intramuscular implantation in rats (Gbureck et al., 2007a) and in goats (Habibovic et al., 2008).

Torres et al. (2011) used monetite monolithic discs-shaped blocks for vertical bone augmentation procedures in a rabbit calvaria model. 3D printed monetite onlays were also used in a rat calvaria bone model by Tamimi et al. (2014). After printing, the cleaned samples were stored in the binder solution (20% H_3PO_4 for 3 × 60 s) to increase the degree of reaction to brushite; they were then concurrently dehydrated into monetite and sterilized by autoclaving (Torres et al., 2011; Tamimi et al., 2014; Habibovic et al., 2008; Gbureck et al., 2007a).

A similar manufacturing procedure was also carried out at room temperature by Klammert et al. (2010a) to produce monetite customized caraniofacial bone grafts to fill bony defects generated using a human cadaver skull.

According to Castilho et al. (2013), a reaction between the TCP powder and the diluted phosphoric acid at room temperature led to the

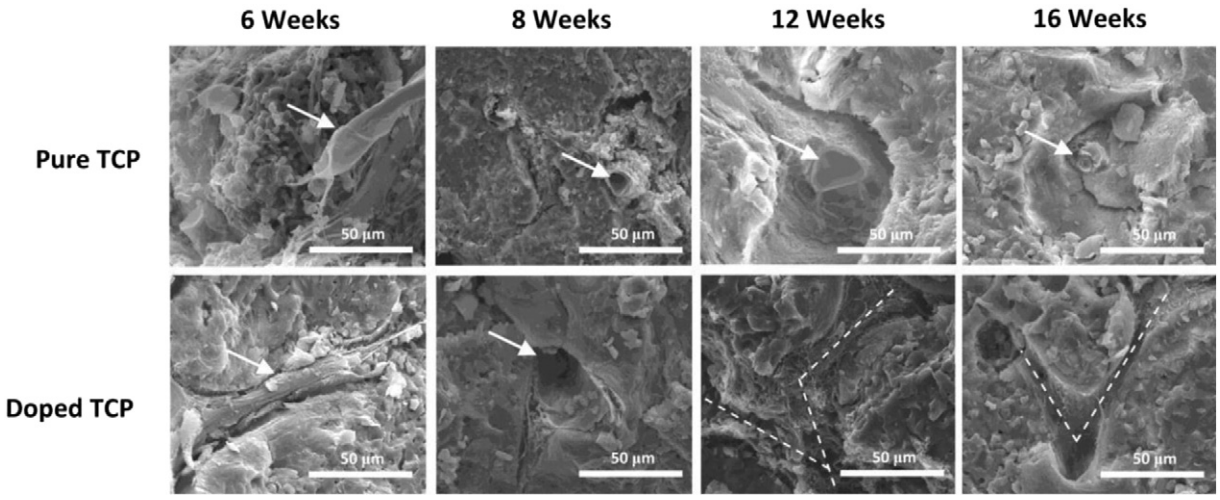

Fig. 4. Field emission scanning electron microscope (FESEM) micrographs of 3D printed pure TCP and SiO_2/ZnO doped TCP scaffolds implanted into a murine femoral defect model. Figures show new blood vessel formation. Arrows indicate blood vessels. Dotted lines show vascular branching pathways formed in the samples. Figure from Fielding and Bose (2013).

formation of brushite samples. After printing, the scaffolds which were posthardened in a binder solution (1 × 30 s), showed mechanical properties in accordance with the strength and stiffness of cancellous bone regardless of the printing direction. Scaffolds printed in the *y* direction presented higher mechanical properties compared to those printed in the axial one aligned with *x*- or *z*-axis of the printing chamber. The anisotropic behavior of 3D printed scaffolds with different failure mechanisms along the *x*- and *y*-axes were also described by Cox et al. (2015), who reported that the scaffolds printed along the y-axis exhibited higher yield and ultimate compressive strength. These results contrasted with those produced by Farzadi et al. (2014), according to whom samples printed in the *x* orientation presented higher compressive strength and modulus with respect to those printed in the *y* and *z* directions.

A customized low temperature CaP scaffold was also used for tibial tuberosity advancement in a dog model; the clinical outcome was good in this case and limb function was completely restored (Castilho et al., 2014b). *In vitro* characterization of the samples was performed prior to implantation. As in the previous study (Castilho et al., 2013), the samples were produced using TCP powder and phosphoric acid binder and posthardened in a binder solution. Posthardening in this case was followed by gamma sterilization. As demonstrated by x-ray diffraction analysis, they were mainly composed of brushite, unreacted TCP β- and α-TCP powder with small amounts of monetite. The samples were found to tolerate high compressive loads while they were sensitive to tensile or flexural stresses.

Low temperature 3D powder-printed CaP composites were also produced by Inzana et al. (2014). The samples were all post-processed by flash dipping in phosphoric acid solution. Supplementing the binder solution (8.75 wt.% phosphoric acid + 0.25 wt.% Tween 80) with collagen significantly improved the strength of 3D printed CaP scaffolds as a linear function of the collagen concentration. Alternatively, scaffolds printed without collagen in the binder solution and coated with 0.5 wt.% neutralized collagen showed increased maximum flexural strength as well as toughness.

Low temperature 3D powder-printed magnesium ammonium phosphate (struvite) structures were also investigated (Klammert et al., 2010b). Pure and 20% diammonium hydrogenphosphate (DAHP)-modified farringtonite samples were tested. Modifying the powder, which was blended with 20% DAHP, was found to improve the cement conversion rate from farringtonite to struvite and thus its mechanical properties. Post-hardening treatment by immersion in the binder solution for 24 h further markedly increased the compressive strength of both pure and DAHP-modified specimens. Depending on the scaffolds' post-treatment, compressive strengths ranged between 2–7 MPa.

Further studies are warranted in view of conflicting requirements of high porosity, which is fundamental for bone tissue ingrowth, and the mechanical integrity of bone graft substitutes. Post-processing approaches can modify and increase the mechanical strength of ceramic porous scaffolds. Improved mechanical properties can be achieved, in particular, by sintering the scaffolds. Microwave sintering may represent a potential alternative to conventional sintering in electric furnaces that offers the advantages of reduced processing times and costs and enhanced reaction and sintering rates. As alternatives to 3D printed CaP structures, especially when high mechanical properties are required in large bone defects, also scaffolds with porous interconntected architecture made of titanium alloys fabricated by additive manufacturing technologies and showing high fatigue strength can be considered (Zhao et al., 2016; Nune et al., 2014, 2015a, 2015b; Li et al., 2016).

High temperatures during the sintering phase are nevertheless counterproductive to incorporating heat-labile molecules, such as drugs, proteins, or growth factors. It is thought that low temperature 3D printing will be able to overcome the limitations of the sintering process which requires high temperatures and thus precludes the incorporation of several bioactive molecules that could stimulate bone formation and reduce graft infections.

3.2.4. Clinical applications/customized scaffolds

Advanced 3D printing technologies can be applied to potentially tailor material/s to the 3D shape of complex critical-sized bone defects. Combining synthetic bone substitutes, such as calcium phosphates, using direct 3D printing technologies may constitute a valid alternative to autogenous bone blocks harvested from intra- or extra-oral sites used to restore large alveolar bone defects that enables immediate or delayed implant placement (Tamimi et al., 2014; Torres et al., 2011).

3D printed scaffolds have been assessed not only *in vitro* but also *in vivo*; monetite (a calcium phosphate material) scaffolds, fabricated *via* low temperature 3D printing, have been investigated in ectopic models of intramuscular implantation in rats (Gbureck et al., 2007a) and in goats (Habibovic et al., 2008).

Monetite onlays, which may be suitable for vertical alveolar bone augmentation procedures, can, moreover, be produced following customized designs using direct 3D printing. Torres et al. (2011) used monetite monolithic discs-shaped blocks for vertical bone augmentation procedures in a rabbit calvaria model. The fact that no damage or fracture to the monetite blocks was noted during screw fixation

would confirm the mechanical quality of those blocks that proved to be neither brittle nor fragile. The lateral end of the blocks, the area between the original calvaria surface and the superior surface of the grafts which has the best blood supply, achieved the highest percentage of bone height. This finding highlighted the importance of a graft's vascularization to achieve more abundant bone formation. Despite heterogeneous new bone formation within the scaffold, eight weeks after surgery the authors reported a total percentage of new bone of 40% and 37% using, respectively, 3.0-mm and 4.0-mm high monetite blocks. These findings are similar to those described in a previous study according to which monetite onlays used for vertical bone augmentation were infiltrated by new bone, occupying up to 43% of the graft volume 8 weeks after implantation time (Tamimi et al., 2009).

3D printed monetite onlays were also used in a rat calvaria bone model by Tamimi et al. (2014). Just as in the study by Torres et al. (2011), customized monetite blocks provided an additional bone height of almost 4 mm when placed on the calvaria bone (2 mm thickness). The authors thus speculated that the vertical bone augmentation achieved using monetite blocks in these animal models could be indicative of the technology's potential to augment a severely resorbed mandible for dental implant placement. Four weeks after delayed dental implant placement in the onlays, histological observations and histomorphometrical analysis revealed, moreover, that the surface of titanium (Ti) implants was partially osseointegrated reaching a bone to implant contact ratio of 37.8 ± 9.9%.

3D printed monetite scaffolds were found to be suitable to manufacture customized site-specific bone substitutes even in an *ex vivo* study (Klammert et al., 2010a). After CT scans were acquired of skull bone defects, specimens were designed with a CAD software and imported into the 3D printing software in a STL file format. The printed scaffolds that were then inserted into the skull defects and fixed with miniplates showed dimensional precision and satisfactory accuracy of fitting.

A CaP customized porous biodegradable scaffold produced by low temperature 3D printing was successfully implanted in a dog model to treat a cruciate ligament rupture (Castilho et al., 2014b). In accordance with preliminary *in vitro* tests (Castilho et al., 2013), the scaffold was fabricated with the higher compressive forces *in vivo* aligned with the printer's *y*-axis to ensure greater mechanical properties in that direction. Sixteen weeks after surgery, the dog's limb function had been recovered and x-ray micrographs confirmed excellent stability of the osteotomy gap. The 3D printed cage, composed of brushite, TCP, and monetite, presented a significant reduction in the x-ray micrograph's projection areas between days 1 and 16 weeks after implantation, suggesting scaffold resorption and bone replacement.

Another study evaluated *in vivo* the regenerative potential of CaP scaffolds fabricated by low temperature 3D printing in a 2 mm critically sized murine femoral defect (Inzana et al., 2014). As demonstrated by the partial replacement and incorporation of these scaffolds into the newly forming bone, the study confirmed that the resorbable scaffolds were osteoconductive. X-ray analysis and 3D micro-CT scans 9 weeks postoperatively demonstrated similar levels of new bone formation in the allografts, in the 3D printed CaP scaffolds, and in the 3D printed CaP scaffold with 1 wt.% collagen dissolved into the binder solution. Collagen coated 3DP samples appeared, instead, to be associated with less new bone formation.

Sintered CaP scaffolds were successfully engineered in one animal study to regenerate bone defects *in vivo* (Tarafder et al., 2013a). Three-D printed and microwave sintered TCP blocks with designed interconnected macropores were implanted in femoral bone defects in a rat model. Histological evaluations carried out 2 weeks after implantation detected osteoid-like bone formation.

Microwave sintered SrO–MgO doped TCP scaffolds showed, moreover, better *in vivo* biological performance with respect to pure TCP when tested in a rat femoral defect model (Tarafder et al., 2013b) as well as in a rabbit femoral condyle defect model (Tarafder et al., 2015).

Other dopants can also be successfully added to TCP powder to enhance the biological response *in vivo* (Fielding and Bose, 2013). Confirmed by von Willebrand factor staining and field emission scanning electron microscopy images, doped samples have been found to induce higher and more complex blood vessel formation with respect to pure samples. While doped samples showed a significant increase in early phase osteogenesis with respect to pure samples, both groups showed nearly complete infiltration of mineralized bone tissue 12 weeks later, and differences between the samples were difficult to detect. The increased rate of bone regeneration was probably linked to the addition of dopants.

Based on these observations, it can be concluded that fabrication of 3D printed customized scaffolds is a promising approach to restore large bone defects. Further efforts should be made to produce patient-specific bone graft substitutes with an optimal osteoconductive microporous structure and an anatomical shape precisely matching the patient's bone defect. Acquisition of precise anatomical data is critical as far as the production workflow is concerned. CT data, CAD and rapid prototyping (RP) technologies can be utilized together to create complex personalized bone tissue engineering scaffolds (Yao et al., 2015). In view of these promising results, further preclinical and clinical human trials are advocated.

3.2.5. Growth factor and drug delivery using powder-based 3d printed scaffolds

A major focus of research has concerned the clinical application of osteoinductive GFs to promote new bone formation. There are many GFs investigated for bone tissue engineering applications, such bone morphogenic proteins (BMPs), vascular endothelial growth factor (VEGF), and fibroblast growth factors (FGFs) (Sivolella et al., 2013).

The localized delivery of GFs from scaffolds fabricated by additive manufacturing has recently attracted significant attention (Kumar et al., 2016b; Nune et al., 2016; Bose et al., 2013), due to the possibility to better control GF orientation and release, than when they are loaded in other vehicles, such as functional hydrogels (Du et al., 2015). Several AM technologies have been used in 3D bioprinting, in particular the ones based on extrusion processes (Du et al., 2015).

Moreover, bone scaffolds obtained by AM have been investigated for the purpose of tuberculosis treatment and also in bone replacement surgeries to avoid internal infections and post-surgery complications (Inzana et al., 2015; Li et al., 2015; Zhu et al., 2015).

3D printed scaffolds have also been used as GF and antimicrobial drug delivery systems and adsorption/desorption behavior of drugs in 3D powder printed calcium phosphate matrices has been investigated (Becker et al., 2012; Gbureck et al., 2007a, 2007b; Cornelsen et al., 2013; Kumar et al., 2016b).

Becker et al. (2012) evaluated heterotopic bone formation on a 3D printed HA scaffold in a rat model, comparing delayed application of BMP-2 at different intervals to the simultaneous placement of the scaffold together with the BMP-2.

Gbureck et al. (2007b) investigated the adsorption and desorption behavior of vancomycin hydrochloride, ofloxacin and tetracycline hydrochloride with brushite, monetite and HA scaffolds fabricated using a 3D powder printing. Also Cornelsen et al. (2013) *in vitro* studied 3D printed TCP scaffolds loaded by infiltration with biodegradable polymers and a model biomolecule in order to provide scaffolds with a sustained drug release function.

Recent advances in 3D printing allowed to load drugs within the matrix. High temperatures during the sintering phase of 3D printed CaP scaffolds can obliterate the bioactivity of incorporated heat-labile molecules. In contrast, low temperature 3D printing allowed spatial distribution of vancomycin within the printed geometry (Vorndran et al., 2010).

In a more recent work, Inzana et al. (2015) didn't used a highly acidic binder (20 wt.% phosphoric acid) as Vorndran et al. (2010), which may result in residual acidity that can be highly cytotoxic (Inzana et al.,

2014), and can significantly degrade the bactericidal activity of the incorporated drug. They utilized a low acidity binder solution to enable low-temperature 3D printing of vancomycin- and rifampin-laden CaP scaffold while maintaining the bactericidal activity (Inzana et al., 2015).

These studies show that 3D printed CaP scaffolds may represent a valuable drug delivery system for bone tissue engineering applications. Further studies are needed to better control the incorporation and release of GFs and drugs from 3D printed bone substitute. Low temperature 3D printing seems to overcome the limitations of the sintering process, which precludes the incorporation of several heat-labile bioactive molecules that could promote bone formation and reduce graft infections.

4. Conclusions

The current state of art concerning powder-based 3DP for bone tissue engineering has been reviewed and discussed here.

In vitro and *in vivo* investigations examining 3D printed scaffolds have uncovered promising results confirming their utility for bone regeneration. CaP ceramics appear to be particularly attractive materials for tissue engineering. There are still, however, many unanswered questions concerning critical aspects linked to depowdering and the cytocompatibility and osteoconductive properties of bone substitutes produced using 3D printing technology. Further studies focusing on critical-sized bone defects are warranted to gain more detailed knowledge about potential clinical applications. This approach, in fact, has opened the way to fabricating customized bone scaffolds with complex internal and external structures that exactly mirror the dimensions of bone defects.

Acronyms

3DP	three-dimensional printing
3D	tridimensional
AM	additive manufacturing
BCP	biphasic calcium phosphate
BMP	bone morphogenic protein
CAD/CAM	computer-aided design and computer aided manufacturing
CaP	calcium phosphate
CT	computed tomography
DAHP	diammonium hydrogenphosphate
FDM	fused deposition modeling
FGF	fibroblast growth factor
GF	growth factor
HA	hydroxyapatite
LDH	lactate dehydrogenase
MSTL	microstereolithography
MTT	3-(4.5-dimethylthiazol-2-yl)-2.5-diphenyltetrazolium bromide
NBCA	α-n-butyl cyanoacrylate
PBS	phosphate buffered saline
PCL	polycaprolactone
PDL	poly(D,L-lactide)
PLGA	polylactic-co-glycolicacid
PPF	polypropylene fumarate
PVOH	Poly(vinyl)alcohol
RP	rapid prototyping
SEM	scanning electron microscope
SFF	solid free-form fabrication
SLA	stereolithography
SLS	selective laser sintering
TCP	tricalciumphosphate
TMC	trimethylene carbonate
VEGF	vascular endothelial growth factor
WST	water-soluble tetrazolium salt

Acknowledgments

The authors have no conflict of interests to declare.

References

Araújo, M.G., Sonohara, M., Hayacibara, R., Cardaropoli, G., Lindhe, J., 2002. Lateral ridge augmentation by the use of grafts comprised of autologous bone or a biomaterial. An experiment in the dog. J. Clin. Periodontol. 29, 1122–1131.
Athanasiou, K.A., Zhu, C., Lanctot, D.R., Agrawal, C.M., Wang, X., 2000. Fundamentals of biomechanics in tissue engineering of bone. Tissue Eng. 6, 361–381.
Becker, S.T., Bolte, H., Schünemann, K., Seitz, H., Bara, J.J., Beck-Broichsitter, B.E., Russo, P.A., Wiltfang, J., Warnke, P.H., 2012. Endocultivation: the influence of delayed vs. simultaneous application of BMP-2 onto individually formed hydroxyapatite matrices for heterotopic bone induction. Int. J. Oral Maxillofac. Surg. 41, 1153–1160.
Bose, S., Dasgupta, S., Tarafder, S., Bandyopadhyay, A., 2010. Microwave-processed nanocrystallinehydroxyapatite: simultaneous enhancement of mechanical and biological properties. Acta Biomater. 6, 3782–3790.
Bose, S., Vahabzadeh, S., Bandyopadhyay, A., 2013. Bone tissue engineering using 3D printing. Mater. Today 16, 496–504.
Bressan, E., Carraro, A., Ferroni, L., Gardin, C., Sbricoli, L., Guazzo, R., Stellini, E., Roman, M., Pinton, P., Sivolella, S., Zavan, B., 2013. Nanotechnology to drive stem cell commitment. Nanomedicine (London) 8, 469–486.
Bressan, E., Ferroni, L., Gardin, C., Sbricoli, L., Gobbato, L., Ludovichetti, F.S., Tocco, I., Carraro, A., Piattelli, A., Zavan, B., 2014. Graphene based scaffolds effects on stem cells commitment. J. Transl. Med. 12, 296.
Butscher, A., Bohner, M., Hofmann, S., Gauckler, L., Müller, R., 2011. Structural and material approaches to bone tissue engineering in powder-based three-dimensional printing. Acta Biomater. 7, 907–920.
Butscher, A., Bohner, M., Doebelin, N., Hofmann, S., Müller, R., 2013. New depowdering-friendly designs for three-dimensional printing of calcium phosphate bone substitutes. Acta Biomater. 9, 9149–9158.
Castilho, M., Dias, M., Gbureck, U., Groll, J., Fernandes, P., Pires, I., Gouveia, B., Rodrigues, J., Vorndran, E., 2013. Fabrication of computationally designed scaffolds by low temperature 3D printing. Biofabrication 5, 035012.
Castilho, M., Moseke, C., Ewald, A., Gbureck, U., Groll, J., Pires, I., Teßmar, J., Vorndran, E., 2014a. Direct 3D powder printing of biphasic calcium phosphate scaffolds for substitution of complex bone defects. Biofabrication 6, 015006.
Castilho, M., Dias, M., Vorndran, E., Gbureck, U., Fernandes, P., Pires, I., Gouveia, B., Armés, H., Pires, E., Rodrigues, J., 2014b. Application of a 3D printed customized implant for canine cruciate ligament treatment by tibial tuberosity advancement. Biofabrication 6, 025005.
Chia, H.N., Wu, B.M., 2015. Recent advances in 3D printing of biomaterials. J. Biol. Eng. 9, 4.
Chiapasco, M., Zaniboni, M., 2009. Clinical outcomes of GBR procedures to correct peri-implant dehiscences and fenestrations: a systematic review. Clin. Oral Implants Res. 20, 113–123.
Chiapasco, M., Zaniboni, M., Rimondini, L., 2007. Autogenous onlay bone grafts vs. alveolar distraction osteogenesis for the correction of vertically deficient edentulous ridges: a 2–4-year prospective study on humans. Clin. Oral Implants Res. 18, 432–440.
Cornelsen, M., Petersen, S., Dietsch, K., Rudolph, A., Schmitz, K., Sternberg, K., Seitz, H., 2013. Infiltration of 3D printed tricalciumphosphate scaffolds with biodegradable polymers and biomolecules for local drug delivery. Biomed. Tech. 58, 4090–4091.
Cox, S.C., Thornby, J.A., Gibbons, G.J., Williams, M.A., Mallick, K.K., 2015. 3D printing of porous hydroxyapatite scaffolds intended for use in bone tissue engineering applications. Mater. Sci. Eng. C Mater. Biol. Appl. 47, 237–247.
Detsch, R., Mayr, H., Ziegler, G., 2008. Formation of osteoclast-like cells on HA and TCP ceramics. Acta Biomater. 4, 139–148.
Detsch, R., Schaefer, S., Deisinger, U., Ziegler, G., Seitz, H., Leukers, B., 2011. In vitro: osteoclastic activity studies on surfaces of 3D printed calcium phosphate scaffolds. J. Biomater. Appl. 26, 359–380.
Du, M., Chen, B., Meng, Q., Liu, S., Zheng, X., Zhang, C., Wang, H., Li, H., Wang, N., Dai, J., 2015. 3D bioprinting of BMSC-laden methacrylamide gelatin scaffolds with CBD-BMP2-collagen microfibers. Biofabrication 7, 044104.
Esposito, M., Grusovin, M.G., Felice, P., Karatzopoulos, G., Worthington, H.V., Coulthard, P., 2009. The efficacy of horizontal and vertical bone augmentation procedures for dental implants — a Cochrane systematic review. Eur. J. Oral Implantol. 2, 167–184.
Farzadi, A., Solati-Hashjin, M., Asadi-Eydivand, M., Abu Osman, N.A., 2014. Effect of layer thickness and printing orientation on mechanical properties and dimensional accuracy of 3D printed porous samples for bone tissue engineering. PLoS One 9, e108252.
Farzadi, A., Waran, V., Solati-Hashjin, M., Rahman, Z.A.A., Asadi, M., Abu Osman, N.A.A., 2015. Effect of layer printing delay on mechanical properties and dimensional accuracy of 3D printed porous prototypes in bone tissue engineering. Ceram. Int. 41, 8320–8330.
Felice, P., Marchetti, C., Iezzi, G., Piattelli, A., Worthington, H., Pellegrino, G., Esposito, M., 2009a. Vertical ridge augmentation of the atrophic posterior mandible with interpositional bloc grafts: bone from the iliac crest vs. bovine anorganic bone. Clinical and histological results up to one year after loading from a randomized-controlled clinical trial. Clin. Oral Implants Res. 20, 1386–1393.
Felice, P., Checchi, V., Pistilli, R., Scarano, A., Pellegrino, G., Esposito, M., 2009b. Bone augmentation versus 5-mm dental implants in posterior atrophic jaws. Four-month post-loading results from a randomised controlled clinical trial. Eur. J. Oral Implantol. 2, 267–281.
Ferroni, L., Gardin, C., Sivolella, S., Brunello, G., Berengo, M., Piattelli, A., Bressan, E., Zavan, B., 2015. A hyaluronan-based scaffold for the in vitro construction of dental pulp-like tissue. Int. J. Mol. Sci. 16, 4666–4681.

Fielding, G., Bose, S., 2013. SiO_2 and ZnO dopants in three-dimensionally printed tricalcium phosphate bone tissue engineering scaffolds enhance osteogenesis and angiogenesis in vivo. Acta Biomater. 9, 9137–9148.
Fielding, G.A., Bandyopadhyay, A., Bose, S., 2012. Effects of silica and zinc oxide doping on mechanical and biological properties of 3D printed tricalcium phosphate tissue engineering scaffolds. Dent. Mater. 28, 113–122.
Fiocco, L., Elsayed, H., Ferroni, L., Gardin, C., Zavan, B., Bernardo, E., 2015. Bioactive wollastonite-diopside foams from preceramic polymers and reactive oxide fillers. Materials 8, 2480–2494.
Gardin, C., Ferroni, L., Favero, L., Stellini, E., Stomaci, D., Sivolella, S., Bressan, E., Zavan, B., 2012. Nanostructured biomaterials for tissue engineered bone tissue reconstruction. Int. J. Mol. Sci. 13, 737–757.
Gardin, C., Ricci, S., Ferroni, L., Guazzo, R., Sbricoli, L., De Benedictis, G., Finotti, L., Isola, M., Bressan, E., Zavan, B., 2015. Decellularization and delipidation protocols of bovine bone and pericardium for bone grafting and guided bone regeneration procedures. PLoS One 10, e0132344.
Gbureck, U., Hozel, T., Klammert, U., Wurzler, K., Muller, F.A., Barralet, J.E., 2007a. Resorbable dicalcium phosphate bone substitutes prepared by 3D powder printing. Adv. Funct. Mater. 17, 3940–3945.
Gbureck, U., Vorndran, E., Müller, F.A., Barralet, J.E., 2007b. Low temperature direct 3D printed bioceramics and biocomposites as drug release matrices. J. Control. Release 122, 173–180.
Habibovic, P., Gbureck, U., Doillon, C.J., Bassett, D.C., van Blitterswijk, C.A., Barralet, J.E., 2008. Osteoconduction and osteoinduction of low-temperature 3D printed bioceramic implants. Biomaterials 29, 944–953.
Hsu, S.H., Yen, H.J., Tseng, C.S., Cheng, C.S., Tsai, C.L., 2007. Evaluation of the growth of chondrocytes and osteoblasts seeded into precision scaffolds fabricated by fused deposition manufacturing. J. Biomed. Mater. Res. B Appl. Biomater. 80, 519–527.
Hutmacher, D.W., Schantz, T., Zein, I., Ng, K.W., Teoh, S.H., Tan, K.C., 2001. Mechanical properties and cell cultural response of polycaprolactone scaffolds designed and fabricated via fused deposition modeling. J. Biomed. Mater. Res. 55, 203–216.
Hutmacher, D.W., Schantz, J.T., Lam, C.X., Tan, K.C., Lim, T.C., 2007. State of the art and future directions of scaffold-based bone engineering from a biomaterials perspective. J. Tissue Eng. Regen. Med. 1, 245–260.
Idaszek, J., Bruinink, A., Święszkowski, W., 2015. Ternary composite scaffolds with tailorable degradation rate and highly improved colonization by human bone marrow stromal cells. J. Biomed. Mater. Res. A 103, 2394–2404.
Ikuta, K., Hirowatari, K., Ogata, T., 1994. Three dimensional micro integratedfluidsystems (MIFS) fabricated by stereo lithography. Micro ElectroMechanical Systems, 1994, MEMS'94, Proceedings, IEEE Workshop on. IEEE, pp. 1–6.
Inzana, J.A., Olvera, D., Fuller, S.M., Kelly, J.P., Graeve, O.A., Schwarz, E.M., Kates, S.L., Awad, H.A., 2014. 3D printing of composite calcium phosphate and collagen scaffolds forbone regeneration. Biomaterials 35, 4026–4034.
Inzana, J.A., Trombetta, R.P., Schwarz, E.M., Kates, S.L., Awad, H.A., 2015. 3D printed bioceramics for dual antibiotic delivery to treat implant-associated bone infection. Eur. Cell. Mater. 30, 232–247.
Kim, J.Y., Jin, G.Z., Park, I.S., Kim, J.N., Chun, S.Y., Park, E.K., Kim, S.Y., Yoo, J., Kim, S.H., Rhie, J.W., Cho, D.W., 2010. Evaluation of solid free-form fabrication-based scaffolds seeded with osteoblasts and human umbilical vein endothelial cells for use in vivo osteogenesis. Tissue Eng. A 16, 2229–2236.
Kim, J., McBride, S., Tellis, B., Alvarez-Urena, P., Song, Y.H., Dean, D.D., Sylvia, V.L., Elgendy, H., Ong, J., Hollinger, J.O., 2012. Rapid-prototyped PLGA/β-TCP/hydroxyapatite nanocomposite scaffolds in a rabbit femoral defect model. Biofabrication 4, 025003.
Klammert, U., Reuther, T., Jahn, C., Kraski, B., Kübler, A.C., Gbureck, U., 2009. Cytocompatibility of brushite and monetite cell culture scaffolds made by three-dimensional powder printing. Acta Biomater. 5, 727–734.
Klammert, U., Gbureck, U., Vorndran, E., Rödiger, J., Meyer-Marcotty, P., Kübler, A.C., 2010a. 3D powder printed calcium phosphate implants for reconstruction of cranial andmaxillofacial defects. J. Craniomaxillofac. Surg. 38, 565–570.
Klammert, U., Vorndran, E., Reuther, T., Müller, F.A., Zorn, K., Gbureck, U., 2010b. Low temperature fabrication of magnesium phosphate cement scaffolds by 3D powder printing. J. Mater. Sci. Mater. Med. 21, 2947–2953.
Kodama, H., 1981. Automatic method for fabricating a three-dimensionalplastic model with photo-hardening polymer. Rev. Sci. Instrum. 52, 1770–1773.
Korpela, J., Kokkari, A., Korhonen, H., Malin, M., Närhi, T., Seppälä, J., 2013. Biodegradable and bioactive porous scaffold structures prepared using fused deposition modeling. J. Biomed. Mater. Res. B Appl. Biomater. 101, 610–619.
Kumar, A., Nune, K.C., Misra, R.D.K., 2016a. Biological functionality of extracellular matrix-ornamented three-dimensional printed hydroxyapatite scaffolds. J. Biomed. Mater. Res. A 00A. http://dx.doi.org/10.1002/jbm.a.35664 (000–000).
Kumar, A., Nune, K.C., Murr, L.E., Misra, R.D.K., 2016b. Biocompatibility and mechanical behaviour of three-dimensional scaffolds for biomedical devices: process–structure–property paradigm. Int. Mater. Rev. 61, 20–45.
Lee, S.J.J., Sachs, E., Cima, M., 1995. Layer position accuracy in powder-based rapid prototyping. Rapid Prototyp. J. 1, 24–37.
Lee, M., Dunn, J.C., Wu, B.M., 2005. Scaffold fabrication by indirect three-dimensional printing. Biomaterials 26, 4281–4289.
Lee, J.W., Kim, J.Y., Cho, D.W., 2010. Solid free-form fabrication technology and its application to bone tissue engineering. Int. J. Stem Cells 3, 85–95.
Lee, J.Y., Choi, B., Wu, B., Lee, M., 2013. Customized biomimetic scaffolds created by indirect three-dimensional printing for tissue engineering. Biofabrication 5, 045003.
LeGeros, R.Z., Lin, S., Rohanizadeh, R., Mijares, D., LeGeros, J.P., 2003. Biphasic calcium phosphate bioceramics: preparation, properties and applications. J. Mater. Sci. Mater. Med. 14, 201–209.
Li, K., Zhu, M., Xu, P., Xi, Y., Cheng, Z., Zhu, Y., Ye, X., 2015. Three-dimensionally plotted MBG/PHBHHx composite scaffold for antitubercular drug delivery and tissue regeneration. J. Mater. Sci. Mater. Med. 26, 102.
Li, S., Zhao, S., Hou, W., Teng, C., Hao, Y., Li, Y., Yang, R., Misra, R.D.K., 2016. Functionally graded Ti-6Al-4V meshes with high strength and energy absorption. Adv. Eng. Mater. 18, 34–38.
Lipowiecki, M., Ryvolová, M., Töttösi, Á., Kolmer, N., Naher, S., Brennan, S.A., Vázquez, M., Brabazon, D., 2014. Permeability of rapid prototyped artificial bone scaffold structures. J. Biomed. Mater. Res. A 102, 4127–4135.
Mangano, F., Macchi, A., Shibli, J.A., Luongo, G., Iezzi, G., Piattelli, A., Caprioglio, A., Mangano, C., 2014. Maxillary ridge augmentation with custom-made CAD/CAM scaffolds. A1-year prospective study on 10 patients. J. Oral Implantol. 40, 561–569.
Markiewicz, M.R., Bell, R.B., 2011. Modern concepts in computer-assisted craniomaxillofacial reconstruction. Curr. Opin. Otolaryngol. Head Neck Surg. 19, 295–301.
Meakin, J.R., Shepherd, D.E., Hukins, D.W., 2004. Short communication: fused deposition models from CT scans. Br. J. Radiol. 77, 504–507.
Nakai, T., Marutani, Y., 1986. Shaping 3-D solid objects using a UV laser and photopolymer. Conference on Lasers and Electro-Optics. Optical Society of America, p. ME2.
Nune, K.C., Misra, R.D.K., Gaytan, S.M., Murr, L.E., 2014. Biological response of next-generation of 3D Ti–6Al–4V biomedical devices using additive manufacturing of cellular and functional mesh structures. J. Biomater. Tissue Eng. 4, 755–771.
Nune, K.C., Kumar, A., Misra, R., Li, S.J., Hao, Y.L., Yang, R., 2015a. Osteoblast functions in functionally graded Ti-6Al-4V mesh structures. J. Biomater. Appl. http://dx.doi.org/10.1177/0885328215617868 (Epub ahead of print).
Nune, K.C., Misra, R.D.K., Gaytan, S.M., Murr, L.E., 2015b. Interplay between cellular activity and three-dimensional scaffold-cell constructs with different foam structure processed by electron beam melting. J. Biomed. Mater. Res. A 103A, 1677–1692.
Nune, K.C., Kumar, A., Murr, L.E., Misra, R.D., 2016. Interplay between self-assembled structure of bone morphogenetic protein-2 (BMP-2) and osteoblast functions in three-dimensional titanium alloy scaffolds: stimulation of osteogenic activity. J. Biomed. Mater. Res. A 104, 517–532.
Oka, K., Murase, T., Moritomo, H., Goto, A., Sugamoto, K., Yoshikawa, H., 2010. Corrective osteotomy using customized hydroxyapatite implants prepared by preoperative computer simulation. Int. J. Med. Robot. 6, 186–193.
Rahmati, S., Shirazi, F., Baghayeri, H., 2009. Perusing piezoelectric head performance in anew 3-D printing design. Tsinghua Sci. Technol. 14 (S1), 24–28.
Rath, S.N., Strobel, L.A., Arkudas, A., Beier, J.P., Maier, A.K., Greil, P., Horch, R.E., Kneser, U., 2012. Osteoinduction and survival of osteoblasts and bone-marrow stromal cells in 3D biphasic calcium phosphate scaffolds under static and dynamic culture conditions. J. Cell. Mol. Med. 16, 2350–2361.
Raynaud, S., Champion, E., Lafon, J.P., Bernache-Assollant, D., 2002. Calcium phosphate apatites with variable Ca/P atomic ratio III. Mechanical properties and degradation in solution of hot pressed ceramics. Biomaterials 23, 1081–1089.
Rezwan, K., Chen, Q.Z., Blaker, J.J., Boccaccini, A.R., 2006. Biodegradable and bioactive porous polymer/inorganic composite scaffolds for bone tissue engineering. Biomaterials 27, 3413–3431.
Seitz, H., Rieder, W., Irsen, S., Leukers, B., Tille, C., 2005. Three-dimensional printing of porous ceramic scaffolds for bone tissue engineering. J. Biomed. Mater. Res. B Appl. Biomater. 74, 782–788.
Sivolella, S., Stellini, E., Brunello, G., Gardin, C., Ferroni, L., Bressan, E., Zavan, B., 2012. Silver nanoparticles in alveolar bone surgery devices. J. Nanomater. 2012, 15.
Sivolella, S., De Biagi, M., Brunello, G., Ricci, S., Tadic, D., Marinc, C., Lops, D., Ferroni, L., Gardin, C., Bressan, E., Zavan, B., 2013. Delivery systems and role of growth factors for alveolar bone regeneration. In: Andrades, J.A. (Ed.), Dentistry, Regenerative Medicine and Tissue Engineering. InTech, Rijeka, Croatia, pp. 713–741 http://dx.doi.org/10.5772/55580.
Smith, M.H., Flanagan, C.L., Kemppainen, J.M., Sack, J.A., Chung, H., Das, S., Hollister, S.J., Feinberg, S.E., 2007. Computed tomography-based tissue-engineered scaffolds in craniomaxillofacial surgery. Int. J. Med. Robot. 3, 207–216.
Strobel, L.A., Rath, S.N., Maier, A.K., Beier, J.P., Arkudas, A., Greil, P., Horch, R.E., Kneser, U., 2014. Induction of bone formation in biphasic calcium phosphate scaffolds by bone morphogenetic protein-2 and primary osteoblasts. J. Tissue Eng. Regen. Med. 8, 176–185.
Tamimi, F., Torres, J., Kathan, C., Baca, R., Clemente, C., Blanco, L., Lopez Cabarcos, E., 2008. Bone regeneration in rabbit calvaria with novel monetite granules. J. Biomed. Mater. Res. A 87, 980–985.
Tamimi, F., Torres, J., Gbureck, U., Lopez-Cabarcos, E., Bassett, D.C., Alkhraisat, M.H., Barralet, J.E., 2009. Craniofacial vertical bone augmentation: a comparison between 3D printed monolithic monetite blocks and autologous onlay grafts in the rabbit. Biomaterials 30, 6318–6326.
Tamimi, F., Torres, J., Al-Abedalla, K., Lopez-Cabarcos, E., Alkhraisat, M.H., Bassett, D.C., Gbureck, U., Barralet, J.E., 2014. Osseointegration of dental implants in 3D-printed synthetic onlay grafts customized according to bone metabolic activity in recipient site. Biomaterials 35, 5436–5445.
Tamjid, E., Simchi, A., Dunlop, J.W., Fratzl, P., Bagheri, R., Vossoughi, M., 2013. Tissue growth into three-dimensional composite scaffolds with controlled micro-features and nanotopographical surfaces. J. Biomed. Mater. Res. A 101, 2796–2807.
Tarafder, S., Balla, V.K., Davies, N.M., Bandyopadhyay, A., Bose, S., 2013a. Microwave-sintered 3D printed tricalcium phosphate scaffolds for bone tissue engineering. J. Tissue Eng. Regen. Med. 7, 631–641.
Tarafder, S., Davies, N.M., Bandyopadhyay, A., Bose, S., 2013b. 3D printed tricalcium phosphate scaffolds: effect of SrO and MgO doping on in vivo osteogenesis in a rat distal femoral defect model. Biomater. Sci. 1, 1250–1259.
Tarafder, S., Dernell, W.S., Bandyopadhyay, A., Bose, S., 2015. SrO- and MgO-doped microwave sintered 3D printed tricalcium phosphate scaffolds: mechanical properties and

in vivo osteogenesis in a rabbit model. J. Biomed. Mater. Res. B Appl. Biomater. 103, 679–690.
Temple, J.P., Hutton, D.L., Hung, B.P., Huri, P.Y., Cook, C.A., Kondragunta, R., Jia, X., Grayson, W.L., 2014. Engineering anatomically shaped vascularized bone grafts with hASCs and 3D-printed PCL scaffolds. J. Biomed. Mater. Res. A 102, 4317–4325.
Teo, E.Y., Ong, S.Y., Chong, M.S., Zhang, Z., Lu, J., Moochhala, S., Ho, B., Teoh, S.H., 2011. Polycaprolactone-based fused deposition modeled mesh for delivery of antibacterial agents to infected wounds. Biomaterials 32, 279–287.
Tonetti, M.S., Hämmerle, C.H.F., 2008. Advances in bone augmentation to enable dental implant placement: consensus report of the sixth european workshop on periodontology. J. Clin. Periodontol. 35, 168–172.
Torres, J., Tamimi, F., Alkhraisat, M.H., Prados-Frutos, J.C., Rastikerdar, E., Gbureck, U., Barralet, J.E., López-Cabarcos, E., 2011. Vertical bone augmentation with 3D-synthetic monetite blocks in the rabbit calvaria. J. Clin. Periodontol. 38, 1147–1153.
Vaezi, M., Seitz, H., Yang, S., 2013. A review on 3D micro-additive manufacturing technologies. Int. J. Adv. Manuf. Technol. 67, 1721–1754.
Vorndran, E., Klammert, U., Ewald, A., Barralet, J.E., Gbureck, U., 2010. Simultaneous immobilization of bioactives during 3D powder printing of bioceramic drug-release matrices. Adv. Funct. Mater. 20, 1585–1591.
Wang, Y., Wei, Q., Pan, F., Yang, M., Wei, S., 2014. Molecular dynamics simulations for the examination of mechanical properties of hydroxyapatite/poly α-n-butyl cyanoacrylate under additive manufacturing. Biomed. Mater. Eng. 24, 825–833.
Wang, Y., Li, X., Wei, Q., Yang, M., Wei, S., 2015. Study on the mechanical properties of three-dimensional directly binding hydroxyapatite powder. Cell Biochem. Biophys. (Epub ahead of print).
Warnke, P.H., Seitz, H., Warnke, F., Becker, S.T., Sivananthan, S., Sherry, E., Liu, Q., Wiltfang, J., Douglas, T., 2010. Ceramic scaffolds produced by computer-assisted 3D printing and sintering: characterization and biocompatibility investigations. J. Biomed. Mater. Res. B Appl. Biomater. 93, 212–217.
Will, J., Melcher, R., Treul, C., Travitzky, N., Kneser, U., Polykandriotis, E., Horch, R., Greil, P., 2008. Porous ceramic bone scaffolds for vascularized bone tissue regeneration. Mater. Sci. Mater. Med. 19, 2781–2790.
Wiria, F.E., Leong, K.F., Chua, C.K., Liu, Y., 2007. Poly-epsilon-caprolactone/hydroxyapatite for tissue engineering scaffold fabrication via selective laser sintering. Acta Biomater. 3 (1), 1–12 (Jan).
Woodard, J.R., Hilldore, A.J., Lan, S.K., Park, C.J., Morgan, A.W., Eurell, J.A., Clark, S.G., Wheeler, M.B., Jamison, R.D., Wagoner Johnson, A.J., 2007. The mechanical properties and osteoconductivity of hydroxyapatite bone scaffolds with multi-scale porosity. Biomaterials 28, 45–54.
Xia, Y., Zhou, P., Cheng, X., Xie, Y., Liang, C., Li, C., Xu, S., 2013. Selective laser sintering fabrication of nano-hydroxyapatite/poly-ε-caprolactone scaffolds for bone tissue engineering applications. Int. J. Nanomedicine 8, 4197–4213.
Xu, N., Ye, X., Wei, D., Zhong, J., Chen, Y., Xu, G., He, D., 2014. 3D artificial bones for bone repair prepared by computed tomography-guided fused deposition modeling for bone repair. ACS Appl. Mater. Interfaces 6, 14952–14963.
Yadoji, P., Peelamedu, R., Agrawal, D., Roy, R., 2003. Microwave sintering of Ni/Zn ferrites: comparison with conventional sintering. Mater. Sci. Eng. B 98 (3), 269–278.
Yao, Q., Wei, B., Guo, Y., Jin, C., Du, X., Yan, C., Yan, J., Hu, W., Xu, Y., Zhou, Z., Wang, Y., Wang, L., 2015. Design, construction and mechanical testing of digital 3D anatomical data-based PCL-HA bone tissue engineering scaffold. J. Mater. Sci. Mater. Med. 26, 5360.
Yen, H.J., Tseng, C.S., Hsu, S.H., Tsai, C.L., 2009. Evaluation of chondrocyte growth in the highly porous scaffolds made by fused deposition manufacturing (FDM) filled with type II collagen. Biomed. Microdevices 11, 615–624.
Zavan, B., Bressan, E., Sivolella, S., Brunello, G., Gardin, C., Ferrarese, N., Ferroni, L., Stellini, E., 2011. Dental pulp stem cells and tissue engineering strategies for clinical application on odontoiatric field. In: Pignatello, R. (Ed.), Biomaterials Science and Engineering. Intech, Rijeka, Croatia, pp. 339–348 http://dx.doi.org/10.5772/24871.
Zhao, S., Li, S.J., Hou, W.T., Hao, Y.L., Yang, R., Misra, R.D., 2016. The influence of cell morphology on the compressive fatigue behavior of Ti–6Al–4V meshes fabricated by electron beam melting. J. Mech. Behav. Biomed. Mater. 59, 251–264.
Zhou, Z., Buchanan, F., Mitchell, C., Dunne, N., 2014. Printability of calcium phosphate: calcium sulfate powders for the application of tissue engineered bone scaffolds using the 3D printing technique. Mater. Sci. Eng. C Mater. Biol. Appl. 38, 1–10.
Zhu, M., Li, K., Zhu, Y., Zhang, J., Ye, X., 2015. 3D-printed hierarchical scaffold for localized isoniazid/rifampin drug delivery and osteoarticular tuberculosis therapy. Acta Biomater. 16, 145–155.